Nanoengineering mechanically robust aerogels via control of foam morphology

S. O. Kucheyev, T. F. Baumann, C. A. Cox, Y. M. Wang, J. H. Satcher Jr., A. V. Hamza, and J. E. Bradby

Citation: Applied Physics Letters **89**, 041911 (2006); doi: 10.1063/1.2236222
View online: http://dx.doi.org/10.1063/1.2236222
View Table of Contents: http://scitation.aip.org/content/aip/journal/apl/89/4?ver=pdfcov
Published by the AIP Publishing

Nanoengineering mechanically robust aerogels via control of foam morphology

S. O. Kucheyev,[a] T. F. Baumann, C. A. Cox, Y. M. Wang, J. H. Satcher, Jr., and A. V. Hamza
Lawrence Livermore National Laboratory, Livermore, California 94550

J. E. Bradby
Department of Electronic Materials Engineering, The Australian National University, Canberra ACT 0200, Australia

(Received 20 March 2006; accepted 5 June 2006; published online 26 July 2006)

Potential of aerogels for technological applications is often limited by their poor mechanical properties. Here, we demonstrate that alumina aerogel monoliths with excellent mechanical properties can be made by controlling the crystallographic phase, shape, and size of nanoligaments. In particular, we show that thermal processing of aerogels with a morphology of interconnected nanoleaflets causes dehydration and associated curling of the nanoleaflets, resulting in a dramatic improvement of mechanical properties. This study shows an effective way to control mechanical properties of the nanoporous solids that can be synthesized with ligaments having a quasi-two-dimensional shape, such as platelets, ribbons, or leaflets. © *2006 American Institute of Physics*. [DOI: 10.1063/1.2236222]

Aerogels (AGs) are ultralow-density open-cell nanofoams with typical porosities of $\gtrsim 90\%$.[1] In AGs, the morphology of a sol-gel-derived wet gel is maintained after the liquid filling the pores is replaced with air during supercritical drying.[1] With very high surface areas, ultralow densities, and control over the elemental composition of nanoligaments, potential applications of AGs are numerous. These include advanced gas- and biosensors, batteries, catalytic devices, thermal insulators, and low dielectric constant materials for integrated circuits.[1–7] For example, alumina AGs, the subject of this study, are attractive for high performance catalysts, ceramics, and separators,[3,6,7] and alumina AG monoliths are desirable as high-temperature thermal insulators for alloy melt processing and in space applications.[6] However, AGs are notoriously known for their poor mechanical properties (see, for example, Refs. 1 and 6–15). In fact, most non-silica-based AG monoliths with porosities $\gtrsim 95\%$ are very fragile and difficult to handle, which limits their current applications.[6,7]

Although we are not aware of any previous attempts to improve mechanical properties of inorganic non-silica-based AGs, there have been several such studies for silica AGs.[9,11,13–16] One approach involved soaking silica gels in monomers which condense into the necks between the particles.[9] Prakash *et al.*[16] modified silica AGs by covering ligaments with silyl groups, which are chemically inert compared to the hydroxyl groups passivating the surface of typical silica AGs.[10] Other attempts to toughen silica AGs involved adding organic polymer molecules,[13] silica and alumina microfibers,[11] or activated carbon powders.[14] However, in most cases, the apparent improvement of mechanical properties could be largely attributed to an increase in the monolith density as a result of adding cross-linking material.[11,13,14]

Here, we report on an entirely different approach to design mechanically robust AGs by controlling their morphology. We demonstrate that crack-free, alumina AG monoliths with excellent mechanical properties can be achieved by synthesizing foams with a morphology of interconnected *nanoleaflets*. Thermal annealing of such AGs causes controlled material dehydration and associated curling of nanoleaflets, resulting in a significant improvement of mechanical properties.

Four sets of alumina AGs were synthesized, labeled CWE-1, CWE-2, CE, and NE (Table I).[20] Details of the AG synthesis can be found in Ref. 7. The average bulk densities of AGs were determined by measuring the dimensions and mass of monolithic samples. Selected AGs were annealed for 2 h in air at temperatures (T^{ann}) of 500 and 800 °C and remained monolithic and apparently crack-free. The AGs were studied by x-ray diffraction (XRD) and transmission electron microscopy (TEM). All four sets of AGs had Brunauer-Emmett-Teller surface areas of $\sim 700\ \mathrm{m^2\ g^{-1}}$, and annealing at 800 °C resulted in an expected reduction in surface areas to $\sim 300-400\ \mathrm{m^2\ g^{-1}}$.[7]

All AGs were subjected to indentation using a UMIS-2000 nanoindentation system with an ~1-mm-radius sapphire spherical indenter. A series of both continuous and partial load-unload indents (with ~5–10 indents for each loading mode for every sample) was carried out at room temperature. The loading rates were ~1–3 mN/s. Indentation curves for different indents on the same sample were generally reproducible within ~10%. Such relatively large error bars do not affect any of the conclusions of this work and are attributed to effects of surface roughness, which is difficult to measure and control for ultralow-density nanoporous solids. Indentation data were analyzed using the method of Field and Swain[21] to extract the (Meyer) hardness H and elastic modulus E. To verify the E values obtained from nanoindentation, selected samples were also studied with Panametrics Ultrasonic analyzer (model 5052 UA) with 180 kHz center frequency transducers. For such measurements, crack-free AGs were cast in shapes of right cylinders, ~1.2 cm in diameter and ~1.5–3.0 cm in length, with parallel cylinder faces. A procedure from Ref. 8 was used to calculate E from the sound velocities measured.

[a]Electronic mail: kucheyev@llnl.gov

TABLE I. Properties of full-density alumina (Refs. 17–19) and alumina aerogels with nanoleaflet (NL) and string-of-pearls (SP) morphologies. Effective hardness H and elastic modulus E were determined from nanoindentation data for a plastic penetration depth of 5 μm. Values of E given in parentheses were obtained from acoustic velocity measurements.

Sample	Precursor	Solvent	T^{ann} (°C)	Morphology	Phase	Density (mg cm^{-3})	Density (%)	E (MPa)	H (kPa)
CWE-1	$AlCl_3 \cdot 6H_2O$	Water/ethanol	20	NL	Boehmite	48	1.41	1.75	39.10
CWE-1	$AlCl_3 \cdot 6H_2O$	Water/ethanol	500	NL	γ+ boehmite	55	1.62	3.35	144.00
CWE-1	$AlCl_3 \cdot 6H_2O$	Water/ethanol	800	NL	γ	80	2.35	7.18 (12.4)	227.00
CWE-2	$AlCl_3 \cdot 6H_2O$	Water/ethanol	20	NL	Boehmite	60	1.77	4.14 (3.2)	158.00
CE	$AlCl_3 \cdot 6H_2O$	Ethanol	20	NL	Boehmite	130	3.82	5.70	87.80
CE	$AlCl_3 \cdot 6H_2O$	Ethanol	500	NL	γ+ boehmite	150	4.41	9.64	132.00
CE	$AlCl_3 \cdot 6H_2O$	Ethanol	800	NL	γ	240	7.06	80.20	1170.00
NE	$Al(NO_3)_3 \cdot 9H_2O$	Ethanol	20	SP	Diaspore	135	3.97	4.37	103.00
NE	$Al(NO_3)_3 \cdot 9H_2O$	Ethanol	800	SP	γ	200	5.88	4.89	60.20
Alumina	···	···	···	full density	···	3400	100.00	2×10^5	1×10^7

A comparison of Figs. 1(a) and 1(d) illustrates that changing the precursor from $Al(NO_3)_3$ to $AlCl_3$ dramatically changes the morphology of resultant AGs from the well known sting-of-pearls morphology [Fig. 1(d)] to a morphology for which the solid network is made from interconnected nanoleaflets [Fig. 1(a)]. The nanoparticles forming the AG with the string-of-pearls morphology shown in Fig. 1(d) are ~5–10 nm in size, whereas the nanoleaflets shown in Fig. 1(a) are ~10–15 nm wide and ≲100 nm long. This nanoleaflet morphology is common for all our AGs synthesized with the $AlCl_3$ precursor (i.e., CWE-1, CWE-2, and CE AGs). However, our TEM study of CE AGs, for which absolute ethanol was used as a solvent, revealed narrower nanoleaflets (~5 nm wide) than for the case of CWE-1 and CWE-2 AGs [shown in Fig. 1(a)] prepared with a water and ethanol mixture as a solvent (see Table I).

Figures 1(a)–1(c) illustrate that thermal annealing at 500 and 800 °C of CWE-1 AGs (with the nanoleaflet morphology) results in the curling of nanoleaflets. In contrast, our TEM study of NE AGs (with the string-of-pearls morphology) annealed at 800 °C has revealed a negligible change in the size of nanoparticles forming the AG skeleton. In addition, our XRD study has shown that the nanoligaments in all as-prepared AGs with the nanoleaflet morphology (CWE-1, CWE-2, and CE) have the γ-boehmite structure, while AGs with the string-of-pearls morphology (NE) exhibit the α-diaspore structure. Both boehmite and diaspore are structures of AlO(OH),[3] indicating that as-synthesized AGs are monohydroxides. After annealing at 800 °C, ligaments in all AGs dehydrate and recrystallize to the γ-Al_2O_3 structure, as revealed by XRD (see Table I). The crystallographic phase of nanoligaments (studied by XRD) can also explain their shape revealed by TEM (Fig. 1). Indeed, γ-AlO(OH) (boehmite), the phase of struts forming AGs with the nanoleaflet morphology, is a layered structure with the layers held together by hydrogen bonds, while α-AlO(OH) (diaspore) in AGs with the string-of-pearls morphology is not a layered structure.[3]

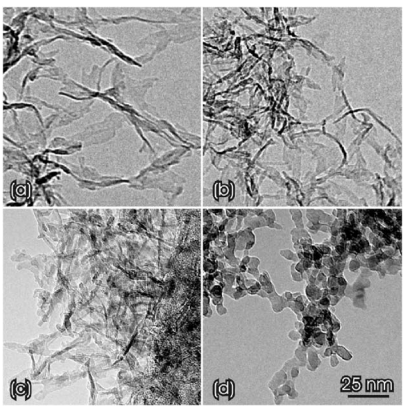

FIG. 1. Bright-field TEM images of CWE-1 [(a)–(c)] and NE (d) aerogels annealed at 20 [(a) and (d)], 500 (b), and 800 °C (c). All four images are of the same magnification.

To illustrate the dramatic effects of the monolith density and foam morphology on mechanical properties of AGs, Fig. 2 shows curves of H (a) and E (b) for four representative AGs as a function of indenter penetration below the circle of contact. Values of E and H for all the samples are given in Table I. In addition, the inset of Fig. 2(a) shows typical continuous load-unload curves for the same four AGs.

The Meyer hardness, defined as the average contact pressure, has different physical meanings for low-density

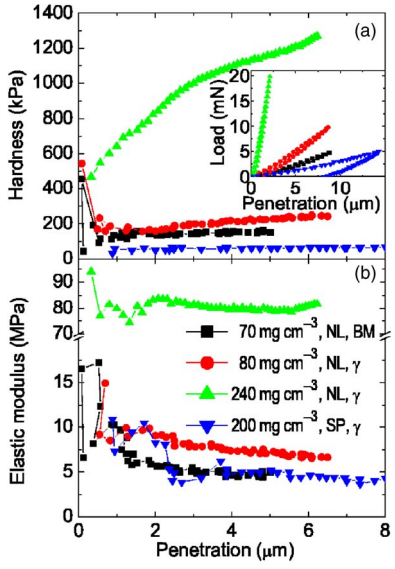

FIG. 2. (Color online) Curves of hardness (a) and elastic modulus (b) as a function of indenter penetration depth, as determined from partial load-unload data, demonstrating the effects of the monolith density, foam morphology, and the phase of nanoligaments on properties of four representative alumina aerogels. Typical continuous load-unload curves for the same four samples are shown in the inset.

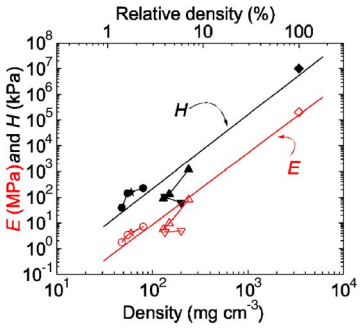

FIG. 3. (Color online) Dependencies of contact pressure (H, closed symbols) and Young's modulus (E, open symbols) on the density of the following sets of aerogels: CWE-1 (circles), CWE-2 (stars), CE (up triangles), and NE (down triangles). Data for full-density alumina are shown by diamonds.

brittle nanoporous solids than for full-density materials. Indeed, the hardness for full-density (nonviscoelastic) solids is defined by fundamental physical processes such as the generation and mobility of dislocations, slip, and/or pressure-induced phase transformations. In contrast, deformation mechanisms in brittle nanofoams (such as alumina AGs) are currently poorly understood[6,8–15] but likely involve elastic bending and brittle fracture of struts, accompanied by the collapse of pores and foam densification. In this case, hardness is determined by the fracture toughness of struts rather than by the dislocation and slip activities or phase transformations as for full-density solids.

It is seen from Fig. 2 that for AGs with the nanoleaflet morphology, both E and H increase with increasing monolith density. More importantly, for a given monolith density, AGs with the nanoleaflet morphology are significantly stiffer and have larger H than AGs with the string-of-pearls morphology. Figure 2(b) also shows that, except for indenter penetration depths $\lesssim 1$ μm affected by surface roughness, E is essentially independent of depth. However, H increases with depth for all the samples [Fig. 2(a)], which we attribute to the effects of strut fracture, associated collapse of pores, and accumulation of the strut material beneath the indentation contact with increasing load.

Table I also shows that our alumina AGs have exceptional mechanical properties. For example, cross-linked "strong" silica-based AGs with densities of $\sim 250-300$ mg cm^{-3}, recently reported by Leventis *et al.*[13], have E of $\sim 5-12$ MPa, which are comparable to values for our alumina AGs with the string-of-pearls morphology of similar densities, but which are an order of magnitude smaller than E for our AGs with the nanoleaflet morphology.

The dependence of H and E on material parameters is more clearly illustrated in Fig. 3. It is seen that both H and E decrease superlinearly with decreasing relative density of AGs, with slopes of 2.9 ± 0.3 and 2.8 ± 0.2, respectively. However, it is clear that data for neither H nor E closely follow a simple power law scaling with a constant exponent. Hence, in addition to the monolith density, other parameters (in particular, the crystallographic phase and shape of ligaments) strongly influence the mechanical properties of the nanofoam. For example, data from Fig. 3 and Table I clearly show that thermal annealing of AGs with the nanoleaflet morphology which causes curling of the nanoleaflets, results in a dramatic improvement of mechanical properties. In contrast, annealing of AGs with the string-of-pearls morphology only slightly increases E but, at the same time, results in a slight reduction in H. Finally, the choice of the solvent during the sol-gel synthesis (which, as discussed above, affects the average width of the nanoleaflets) also affects AG mechanical properties (compare circles and up triangles in Fig. 3). Hence, it would not be appropriate to describe data from Fig. 3 with scaling law models for mechanical properties of porous solids[12,22] since, in addition to the monolith density, other important parameters are variable and strongly affect mechanical characteristics.

The above results demonstrate that both the framework connectivity and the mechanical properties of individual nanoligaments in foams with a nanoleaflet morphology can be improved by thermal processing, which causes dehydration, phase transformation, and associated curling of leaflets.

Work at LLNL was performed under the auspices of the U.S. DOE by the UC, LLNL under Contract No. W-7405-Eng-48. Work at the ANU was supported by the ARC.

[1]See, for example, a review by N. Hüsing and U. Schubert, Angew. Chem., Int. Ed. **37**, 22 (1998).
[2]R. D. Miller, Science **286**, 421 (1999).
[3]P. Euzen, P. Raybaud, X. Krokidis, H. Toulhoat, J. L. L. Loarer, J. P. Jovilet, and C. Froidefont, in *Handbook of Porous Solids*, edited by F. Schuth, K. S. W. Sing, and J. Weitkamp (Wiley-VCH, Weinheim, 2002), p. 1591.
[4]D. R. Rolison, Science **299**, 1698 (2003).
[5]J. L. Mohanan, I. U. Arachchige, and S. L. Brock, Science **307**, 397 (2005).
[6]J. F. Poco, J. H. Satcher, Jr., and L. W. Hrubesh, J. Non-Cryst. Solids **285**, 57 (2001).
[7]T. F. Baumann, A. E. Gash, and J. H. Satcher, Jr., Chem. Mater. **17**, 395 (2005).
[8]J. Gross, G. Reichenauer, and J. Fricke, J. Phys. D **21**, 1447 (1988).
[9]T. Woignier and J. Phalippou, J. Non-Cryst. Solids **100**, 404 (1988).
[10]J. Fricke, Nature (London) **374**, 409 (1995).
[11]K. E. Parmenter and F. Milstein, J. Non-Cryst. Solids **223**, 179 (1998).
[12]H. S. Ma, A. P. Roberts, J. H. Prevost, R. Jullien, and G. W. Scherer, J. Non-Cryst. Solids **227**, 127 (2000).
[13]N. Leventis, C. Sotiriou-Leventis, G. Zhang, and A. M. M. Rawashdeh, Nano Lett. **2**, 957 (2002).
[14]M. Moner-Girona, E. Martinez, J. Esteve, A. Roig, R. Solanas, and E. Molins, Appl. Phys. A: Mater. Sci. Process. **74**, 119 (2002).
[15]E. M. Lucas, M. S. Doescher, D. M. Ebenstein, K. J. Wahl, and D. R. Rolison, J. Non-Cryst. Solids **350**, 244 (2004).
[16]S. S. Prakash, C. J. Brinker, A. J. Hurd, and S. M. Rao, Nature (London) **374**, 439 (1995).
[17]A skeletal density of alumina of 3.4 g cm^{-3} was used to estimate the relative density of AG monoliths since all the three phases of alumina studied here have densities similar to that (3.4, 3.4, and 3.7 g cm^{-3} for boehmite, diaspore, and γ-Al_2O_3, respectively) (Ref. 18). We are also not aware of any reports of E and H measurements for full-density boehmite and diaspore. In Table I, we use $E=200$ GPa and $H=10$ GPa for full-density alumina since these values are representative of full-density γ-Al_2O_3 and amorphous Al_2O_3 (Ref. 19).
[18]*CRC Handbook of Chemistry and Physics*, 84th ed., edited by D. R. Lide (CRC, New York, 2003).
[19]See, for example, T. C. Chou, T. G. Neih, S. D. McAdams, and G. M. Pharr, Scr. Metall. Mater. **25**, 2203 (1991); J. C. Barbour, J. A. Knapp, D. M. Follstaedt, T. M. Mayer, K. G. Minor, and D. L. Linam, Nucl. Instrum. Methods Phys. Res. B **166–167**, 140 (2000).
[20]Note that the only difference in preparation conditions of samples CWE-1 and CWE-2 in Table I was a different concentration of the precursor in the starting solution, resulting in different densities of AG monoliths.
[21]J. S. Field and M. V. Swain, J. Mater. Res. **8**, 297 (1993).
[22]See, for example, L. J. Gibson, and M. F. Ashby, *Cellular Solids* (Cambridge University Press, Cambridge, 1997); D. J. Green and P. Colombo, MRS Bull. **28**, 296 (2003).